

Journal of Materials Chemistry A

Accepted Manuscript



This is an *Accepted Manuscript*, which has been through the Royal Society of Chemistry peer review process and has been accepted for publication.

Accepted Manuscripts are published online shortly after acceptance, before technical editing, formatting and proof reading. Using this free service, authors can make their results available to the community, in citable form, before we publish the edited article. We will replace this *Accepted Manuscript* with the edited and formatted *Advance Article* as soon as it is available.

You can find more information about *Accepted Manuscripts* in the [Information for Authors](#).

Please note that technical editing may introduce minor changes to the text and/or graphics, which may alter content. The journal's standard [Terms & Conditions](#) and the [Ethical guidelines](#) still apply. In no event shall the Royal Society of Chemistry be held responsible for any errors or omissions in this *Accepted Manuscript* or any consequences arising from the use of any information it contains.

Selective Carbon Dioxide Adsorption of ϵ -Keggin-type Zincomolybdate-based Purely-Inorganic 3D Frameworks

Cite this: DOI: 10.1039/x0xx00000x

Received 00th January 2012,
Accepted 00th January 2012

DOI: 10.1039/x0xx00000x

www.rsc.org/

Zhenxin Zhang¹, Masahiro Sadakane^{2,3,*}, Shin-ichiro Noro^{3,4,5}, Toru Murayama¹, Takashi Kamachi⁶, Kazunari Yoshizawa⁶, and Wataru Ueda^{1*}

Polyoxometalate-based 3D frameworks, $\text{Na}_{1.5}\text{H}_{11.4}[\text{ZnMo}_{12}\text{O}_{40}\{\text{Zn}_2\}]\cdot 5.5\text{H}_2\text{O}$ and $(\text{NH}_4)_{1.5}\text{H}_{8.5}[\text{ZnMo}_{12}\text{O}_{40}\{\text{Zn}_2\}]\cdot 6\text{H}_2\text{O}$, are synthesized in moderate yields. Rotation of the reactor under a hydrothermal condition is essential to improve the yield. The materials show a zeolite-like selective molecule adsorption property. Dependent on the micropore aperture size of the materials, small molecules can be adsorbed in the materials, while large molecule cannot. The enthalpy of adsorption and DFT calculation indicate that the materials strongly interact with CO_2 , but weakly interact with CH_4 , due to electrostatic interaction between the materials and molecules. CO_2/CH_4 co-sorption experiments show that the materials can selectively adsorb CO_2 , and CO_2 adsorption selectivity of the material with sodium cation is higher than that of the material with ammonium cation. The material with sodium ion can be utilized for gas chromatographical separation of CH_4 and CO_2 .

CO_2 separation is an important topic from the viewpoints of industrial processes and environmental protection, and many techniques for CO_2 separation have been developed over the past few decades.^{1–5} Generally, there are two kinds of materials for CO_2 separation based on different separation mechanisms. One type of materials for CO_2 separation is based on chemisorption. Such materials include calcium oxide and amine solution. However, these materials have significant disadvantages such as toxicity, corrosiveness, and high energy for regeneration. The second type of materials is based on physical-sorption. Such materials include zeolites and metal-organic frameworks (MOFs), and they are considered to have higher application potential because the corresponding processes are environmentally friendly and economically feasible techniques.

Polyoxometalates (POMs) are metal oxide clusters of early transition metals, such as tungsten, molybdenum, vanadium and niobium, which display characteristic redox and acidic properties, and they therefore have many applications including catalysis, adsorption, separation, electrochemistry, and medicine.^{6–9} In material chemistry, POMs act as building blocks, and inorganic metal oxides can be synthesized on the basis of connection of POMs with other metal ions.^{10–14} POMs

also interact with organic ligands or organic metal complexes to form hybrid materials, including POMOFs^{15–20} and POM-macroocation materials.^{21–29} POM-macroocation materials show interesting adsorption properties.

A novel catalog of POM-based material has recently been synthesized and structurally characterized and is best described

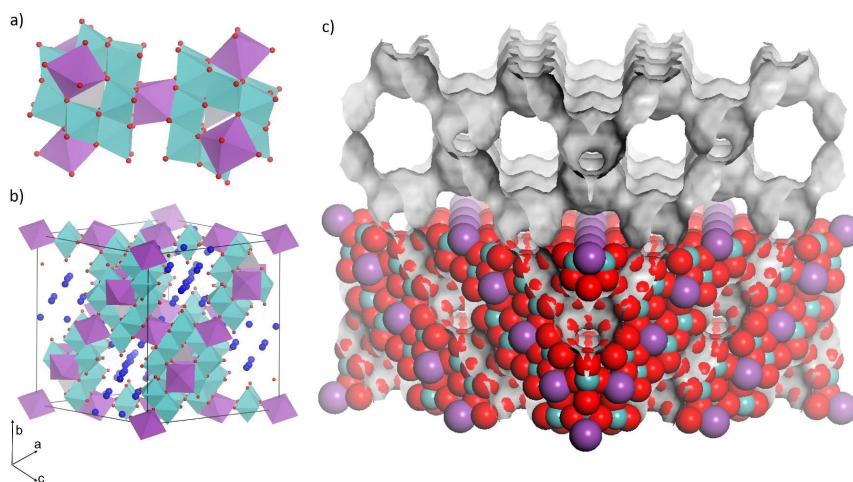


Figure 1. Polyhedral representations of a) ϵ -Keggin POM unit and its connection, b) unit cell of ϵ -Keggin POM-based framework, gray tetrahedron: central Zn-O tetrahedron, blue octahedron: surrounding Mo-O octahedron, purple octahedron: linker Zn-O octahedron, deep blue ball: cation and water, c) CPK (Corey, Pauling, and Koltun) representation of the material with Connelly surface (gray curved surface) that shows the micropore system of the material.

to be fully-inorganic microporous POM-based metal oxides.^{30,31} Frameworks of the materials are comprised of ϵ -Keggin POM with metal ion linkers (Figure 1). The materials show zeolite-like properties such as ion exchange, molecule adsorption, and acid catalysis.

An important property of the POM-based microporous material is its high chemical composition diversity, which allows different kinds of elements to be incorporated in the material. The composition of POM unit, linker ion, and counteraction can be easily changed without altering the basic structure of the material. Several iso-structural materials have been successfully synthesized.³²

Herein, we describe the synthesis of ϵ -Keggin POM-based 3D frameworks composed of $[\text{ZnMo}_{12}\text{O}_{40}]$ and Zn ion linkers with sodium ion or ammonium cation, $\text{Na}_{1.5}\text{H}_{11.4}[\text{ZnMo}_{12}\text{O}_{40}\{\text{Zn}_2\}]\cdot 5.5\text{H}_2\text{O}$ or $(\text{NH}_4)_{1.5}\text{H}_{8.5}[\text{ZnMo}_{12}\text{O}_{40}\{\text{Zn}_2\}]\cdot 6\text{H}_2\text{O}$, denoted as Na–Mo–Zn oxide or NH_4 –Mo–Zn oxide, respectively. We demonstrate the adsorption property of the materials. Small molecules such as CO_2 , CH_4 , and C_2H_6 are adsorbed in the materials, while a large molecule such as C_3H_8 is not adsorbed. CO_2/CH_4 co-sorption experiments showed that the materials selectively adsorb CO_2 from a CO_2/CH_4 mixture. CO_2 adsorption in the materials can be tuned by altering counteractions, and CO_2 separation efficiency can be remarkably enhanced by incorporating sodium ion in the material. The material of Na–Mo–Zn oxide can be used as a material for gas chromatographic separation of CO_2 and CH_4 .

Experimental.

Material synthesis.

Synthesis of Na–Mo–Zn oxide. $\text{Na}_2\text{MoO}_4\cdot 2\text{H}_2\text{O}$ (2.823 g, 11.7 mmol based on Mo) was dissolved in 40 mL of water. Then metal molybdenum (0.2 g, 2.08 mmol) and ZnCl_2 (0.453 g, 3.33 mmol) were added in sequence. The pH value of the precursor solution was adjusted to 4.8 by addition of H_2SO_4 (1 M). The mixture solution was well sealed in an autoclave with a Teflon liner, and the autoclave was fixed in an oven with a mechanical rotation system. Hydrothermal synthesis was performed at 448 K with rotation (1 rpm) for 24 h (see experimental apparatus in supporting information Figure S1). After hydrothermal reaction and cooling of the autoclave, the crude solid was transferred to a 100-mL beaker and 60 mL of water was added. For purification and solid recovery, the mixture was centrifuged (1700 rpm, 2 min), and the suspension (containing the product) solution was separated from the precipitate formed on the bottom after centrifugation. Then after addition of 60 mL of water to the precipitate, the solution was centrifuged and the new upper suspension solution was separated. Addition of water, centrifugation, and separation were carried out two more times. The collected suspension (containing the product) was centrifuged (3500 rpm, 120 min), and solid on the bottom of the centrifugation tube was collected. The collected solid was washed with water by dispersing in 10 mL of water and subsequent centrifugation (3500 rpm, 120 min). After the washing process had been carried out two more times, the obtained solid was dried at 333 K overnight. Then 1.18~1.34 g

of Na–Mo–Zn oxide (yield: 57%~63% based on Mo) was obtained.

Synthesis of NH_4 –Mo–Zn oxide. $(\text{NH}_4)_6\text{Mo}_7\text{O}_{24}\cdot 4\text{H}_2\text{O}$ (2.060 g, 11.7 mmol based on Mo) was dissolved in 40 mL of water. Then metal molybdenum (0.2 g, 2.08 mmol) and ZnCl_2 (0.453 g, 3.33 mmol) were added in sequence. The pH value of the precursor solution was adjusted to 4.8 by addition of H_2SO_4 (1 M). The mixture solution was well sealed in an autoclave with a Teflon liner, and the autoclave was fixed in an oven with a mechanical rotation system. Hydrothermal synthesis was performed at 448 K with rotation (1 rpm) for 24 h. After hydrothermal reaction, the purification process was the same as that for Na–Mo–Zn oxide. Then 1.29~1.46 g of NH_4 –Mo–Zn oxide (yield: 62%~71% based on Mo) was obtained.

Synthesis of NH_4 –Na–Mo–Zn oxide by ion-exchange of Na–Mo–Zn oxide with NH_4^+ . 0.3 g of Na–Mo–Zn oxide was dispersed into 15 mL of water. Then NH_4Cl (0.065 g, 1.21 mmol) was added. The solution was heated at 353 K for 6 h with stirring. The resulting material was separated by filtration, washed by water for 3 times and dried at 333 K overnight.

Elemental Analysis:

Na–Mo–Zn oxide: Calcd for $\text{Na}_{1.5}\text{Zn}_3\text{Mo}_{12}\text{O}_{45.5}\text{H}_{22.4}$: Zn, 9.20; Mo, 53.99; Na, 1.62; H, 1.05, Found: Zn, 9.70; Mo, 53.45; Na, 1.39; H, 0.97.

NH_4 –Mo–Zn oxide: Calcd for $\text{N}_{1.5}\text{Zn}_3\text{Mo}_{12}\text{O}_{46}\text{H}_{26.5}$: Zn, 9.21; Mo, 54.03; N, 0.99; H, 1.24, Found: Zn, 9.25; Mo, 53.95; N, 1.02; H, 1.22.

NH_4 –Na–Mo–Zn oxide: Calcd for $\text{N}_{1.4}\text{Na}_{0.1}\text{Zn}_3\text{Mo}_{12}\text{O}_{45.5}\text{H}_{28}$: Zn, 9.23; Mo, 54.17; Na, 0.11, N, 0.92; H, 1.32, Found: Zn, 9.61; Mo, 54.24; Na, 0.07; N, 1.20; H, 1.39.

Characterization.

Powder X-ray diffraction (XRD) patterns were obtained on RINT2200 (Rigaku) with $\text{Cu K}\alpha$ radiation (tube voltage: 40 kV, tube current: 20 mA). Scanning electron microscopy (SEM) images were obtained with HD-2000 (HITACHI). Transmission electron microscopy (TEM) images were taken with a 200 kV TEM (JEOL JEM-2100F). Temperature-programmed desorption mass spectrometry (TPD-MS) measurements were carried out from 313 K to 893 K at a heating rate of 10 K min^{-1} under helium (flow rate: 50 mL min^{-1}). Samples were set up between two layers of quartz wool. A TPD apparatus (BEL Japan, Inc.) equipped with a quadrupole mass spectrometer (M-100QA; Anelva) was used to detect NH_3 ($m/z = 16$) and H_2O ($m/z = 18$). For TPD-MS measurements of the materials after heat treatment, the samples were heated at 473 K under high vacuum for 2.5 h in a TPD instrument before measurements. After the temperature had been decreased to 373 K, TPD measurement was started. Fourier transform infrared (FT-IR) analysis was carried out on PARAGON 1000, Perkin Elmer. X-ray photoelectron spectroscopy (XPS) was performed on JPS-9010MC (JEOL). The spectrometer energies were calibrated using the C 1s peak at 284.8 eV. Thermal analysis (TG-DTA) was performed on Thermo Plus, TG8120 (Rigaku) under N_2 (200 mL/min).

Elemental compositions were determined by an inductive coupling plasma (ICP-AES) method (ICPE-9000, Shimadzu). CHN elemental composition was determined at Instrumental Analysis Division, Equipment Management Center, Creative Research Institution, Hokkaido University.

Sorption experiments.

Na–Mo–Zn oxide and NH₄–Mo–Zn oxide were calcined at 473 K for 2.5 h under vacuum (denoted as Cal–Na–Mo–Zn oxide and Cal–NH₄–Mo–Zn oxide) before all adsorption experiments.

N₂ sorption isotherms were obtained by a BELSORP MAX (BEL Japan Inc.) sorption analyzer at 77 K. Pore size distribution was calculated by the SF method. Molecule (CO₂, CH₄, C₂H₆, and C₃H₈) adsorption was performed on the materials by a BELSORP MAX (BEL Japan Inc.) sorption analyzer. Adsorption temperature was kept by at 278, 288, and 298 K using a water bath. Surface areas of the materials were calculated from the CO₂ adsorption isotherm by the BET method, and the cross-sectional area of CO₂ was 0.201 nm².³³

CO₂/CH₄ co-sorption measurements were carried out by a multicomponent gas adsorption apparatus, BELSORP VC (BEL Japan Inc.). In this apparatus, the total adsorbed amount was calculated by a constant volume method, and the composition ratio of CO₂ and CH₄ gases in equilibrium was determined using an Agilent 490 Micro gas chromatographic (GC) system equipped with a thermal conductive detector. From these data, we calculated adsorbed amounts and equilibrium partial pressures for each gas. The initial dosing total pressures were set to 14.5 and 278.7 kPa for Cal–Na–Mo–Zn oxide and 14.5 and 279.9 kPa for Cal–NH₄–Mo–Zn oxide. The initial gas proportion was CO₂: CH₄ = 40: 60 (mol). After reaching the equilibrium, a small portion of the gas phase was used for GC analysis, leading to a slight decrease in system total pressure. Then co-sorption measurements were continued by using the residual gas. This process was repeated 5 times for each initial dosing pressure.

The selectivity of CO₂ over CH₄ was calculated by the following equation.

$$S_{\text{CO}_2} = (x_{\text{CO}_2}/y_{\text{CO}_2})/(x_{\text{CH}_4}/y_{\text{CH}_4})$$

y_{CO_2} : mole fraction of component CO₂ in gas phase;

y_{CH_4} : mole fraction of component CH₄ in gas phase;

x_{CO_2} : mole fraction of component CO₂ in adsorbed phase;

x_{CH_4} : mole fraction of component CH₄ in adsorbed phase.

Enthalpy of adsorption calculation. Pure gas adsorption of CO₂ and CH₄ was carried out at different temperatures of 278, 288, and 298 K on the materials (Figure S2–Figure S5). The isotherms of CO₂ and CH₄ were fitted with several adsorption models (Table S1), and it was found that the dual-site Langmuir-Freundlich model was the best model, for which the equation is as follows:

$$q = \frac{q_1 b_1 p^{n_1}}{1 + b_1 p^{n_1}} + \frac{q_2 b_2 p^{n_2}}{1 + b_2 p^{n_2}}$$

where q is adsorbed amount, p is pressure, and q_1 , q_2 , b_1 , b_2 , n_1 , and n_2 are fitting parameters, which are listed in Table S2–Table S5.

The resulting R² values of the fitting processes were quite close to 1, indicating that simulated isotherms by using the dual-site Langmuir-Freundlich model fitted the experimental isotherms well.

The enthalpy of adsorption was calculated by the Clausius-Clapeyron equation using the dual-site Langmuir-Freundlich fitting results.

$$\frac{d \ln p}{dT} = \frac{\Delta H}{RT^2}$$

where p is pressure, T is temperature, and ΔH is enthalpy of adsorption.

GC separation of CO₂ and CH₄. GC separation of a gas mixture of CO₂ and CH₄ using a column packed with Na–Mo–Zn oxide was performed with a Shimadzu GC-8A system equipped with a thermal conductivity detector. Na–Mo–Zn oxide was well grounded and screened with a mesh (aperture: 150 μm), and about 20 mL of Na–Mo–Zn oxide was densely packed into a column (length: 1 m, inner diameter: 3 mm). The fresh column of Na–Mo–Zn oxide was treated at 473 K by introducing a carrier gas of He for 2.5 h to remove the original water in the material and open the micropores of the material. The gas mixture (0.1 mL, CO₂: CH₄ = 1: 1) was injected, and separation was carried out at 363 K.

Structural determination, computer-based simulation, and DFT calculations.

Structural determination of NH₄–Mo–Zn oxide was performed by ab initio structural determination with powder diffraction,³⁴ the detailed process of which is shown in supporting information. Material modeling, X-cell program,³⁵ Pawley refinement, and Rietveld refinement³⁶ were performed with the Materials Studio package (Accelrys Software Inc.). The programs of DICVOL06³⁷ and EdPCR were carried out with the Fullprof package. A charge-flipping algorithm³⁸ was performed with the superflip program in Jana2006, and electron density maps were generated with Chimera 1.8.1.

Monte Carlo simulation was performed to predict the adsorbed structure of the guest molecule in the primitive cell of Cal–Na–Mo–Zn oxide with the adsorption locator program in the Materials studio package. First, the structure of the material, CO₂, and CH₄ were optimized by using the DMol³ program.^{39,40} We employed the Perdew–Burke–Ernzerhof (PBE) generalized gradient functional and DND basis set. Calculated Mulliken atomic charge was applied for Monte Carlo simulation. Partial atomic charges of CO₂ were C = +0.70e and O = -0.35e,⁴¹ and CH₄ was recognized as an electrostatic neutral molecule.⁴² The guest molecules were introduced into the framework of the material one by one.

Results and discussion

Material synthesis and characterization

The synthesis process for Mo–Zn oxides was mainly according to our previous paper.³² However, the previous process produced Na–Mo–Zn oxide with a low yield (14% based on

Mo) with some impurities such as MoO_2 , ZnMoO_4 and Mo (Figure S6), which might have been caused by an insoluble starting material such as metal Mo and the poorly mixed precursor solution. It was known that mixing of solid precursors during reactions change selectivity of products.^{43,44} Here, we applied the dynamic method for material synthesis, in which the reactors were rotated under hydrothermal conditions (Figure S1). In the case of synthesis of Mo–Zn oxides, we found that applying rotation affected the purity and yield of the material. XRD patterns of the crude solids of Na–Mo–Zn oxide and NH_4 –Mo–Zn oxide with and without rotation (Figure S6) indicated that rotation synthesis suppressed the side-reactions and increased the isolated yields of the materials (about 57%–63% based on Mo for Na–Mo–Zn oxide, about 62%–71% based on Mo for NH_4 –Mo–Zn oxide). We carried out the synthesis many times and found the reproducibilities of the synthesis for both materials are very good.

Furthermore, it was found that the rotation speed affected the yields of the materials. Low rotation (1 rpm) speed resulted in high isolated yields for both Mo–Zn oxides, and increasing the rotation speed would decrease the yields of products (Figure S7). The main impurities in crude solids of the materials from the synthesis with different rotation speeds were metal Mo (Figure S6). The amount of metal Mo increased in the crude solid with increase in rotation speed (Figure S6B), which illustrated that high rotation speeds hindered Mo consumption. This might ascribe to our rotation apparatus (Figure S1), in which a centripetal force would be applied to the solid in the solution to make non-uniform mixing of the Mo metal in the solution.

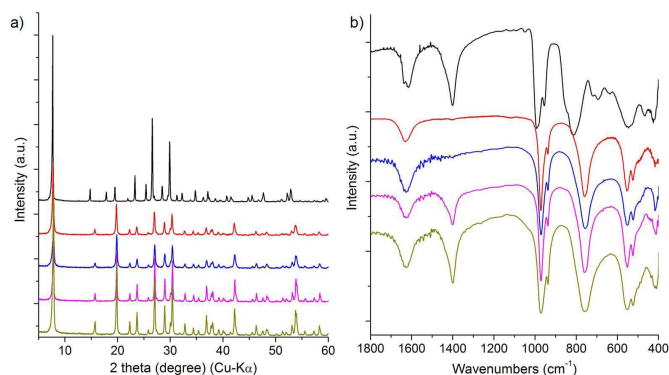


Figure 2. a) Powder XRD patterns of POM-based materials, lattice parameter of Na–Mo–Zn oxide: 19.4675 Å and lattice parameter of NH_4 –Mo–Zn oxide: 19.4533 Å, and b) FT-IR spectra of POM-based materials, black: Mo–V–Bi oxide, red: Na–Mo–Zn oxide using a non-dynamic method,³² blue: Na–Mo–Zn oxide using a dynamic method, purple: NH_4 –Mo–Zn oxide, and yellow: NH_4 –Na–Mo–Zn oxide.

By using different Mo sources with different cations ($\text{Na}_2\text{MoO}_4 \cdot 2\text{H}_2\text{O}$ and $(\text{NH}_4)_6\text{Mo}_7\text{O}_{24} \cdot 4\text{H}_2\text{O}$), materials of Mo–Zn oxide with different counteranions, Na–Mo–Zn oxide and NH_4 –Mo–Zn oxide, were prepared. Elemental analysis indicated that the Na: Mo: Zn ratio of 1.5: 12: 3 of Na–Mo–Zn oxide obtained by the dynamic method that we used was the same as that of Na–Mo–Zn oxide obtained by our last non-dynamic method.³² The NH_4 : Mo: Zn ratio of NH_4 –Mo–Zn oxide was 1.5: 12: 3. XRD patterns and FT-IR spectra (peaks below 1000 cm^{-1} ascribed to the POM moiety) of both materials were similar to those of Mo–V–Bi oxide and Na–Mo–Zn oxide obtained by our last non-dynamic method (Figure 2),^{30,32}

indicating that the structures of materials synthesized by the dynamic method were similar to the structure of the reported Na–Mo–Zn oxide obtained by our last non-dynamic method. SEM images of the resulting materials showed octahedral morphologies typical for ϵ -Keggin-type heteropolyoxometalate-based framework compounds with sizes of the crystallite of 100–300 nm (Figure 3a,b).

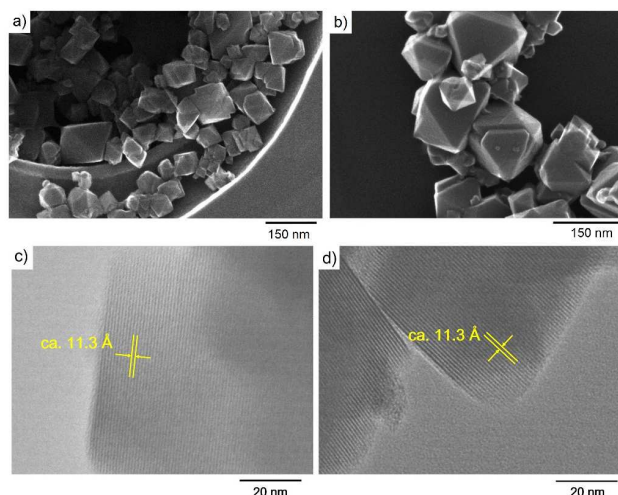


Figure 3. SEM images of a) Na–Mo–Zn oxide and b) NH_4 –Mo–Zn oxide and TEM images of c) Na–Mo–Zn oxide and d) NH_4 –Mo–Zn oxide.

The structure of NH_4 –Mo–Zn oxide was obtained by powder diffraction Rietveld analysis (Figure S8) (detailed process shown in supporting information) combined with elemental analysis, FT-IR, and XPS analysis (Figure S9). The detailed chemical formulas of Na–Mo–Zn oxide and NH_4 –Mo–Zn oxide were estimated to be $\text{Na}_{1.5}\text{H}_{11.4}[\text{Zn}^{\text{II}}\text{Mo}^{\text{VI}}_{11}\text{Mo}^{\text{V}}_{10.9}\text{O}_{40}\{\text{Zn}^{\text{II}}_2\}] \cdot 5.5\text{H}_2\text{O}$ and $(\text{NH}_4)_{1.5}\text{H}_{8.5}[\text{Zn}^{\text{II}}\text{Mo}^{\text{VI}}_{11}\text{Mo}^{\text{V}}_{10}\text{O}_{40}\{\text{Zn}^{\text{II}}_2\}] \cdot 6\text{H}_2\text{O}$, respectively. The frameworks of both materials were formed by assembly of ϵ -Keggin-type zirconomolybdate, $[\text{ZnMo}_{12}\text{O}_{40}]$, where one Zn–O tetrahedron was surrounded by 12 Mo–O octahedra. TEM showed that the distance of (1 1 1) plane was close to each other, indicating that the basic structures of the materials were the same (Figure 3c,d), and in good agreement with the results of structural analysis.

The difference between the two oxides was the counteranion, because cation species of the starting materials were different. The void space surrounded by the frameworks of Na–Mo–Zn oxide and NH_4 –Mo–Zn oxide was occupied with guest species, including water and sodium ion for Na–Mo–Zn oxide and including water and ammonium cation for NH_4 –Mo–Zn oxide, in the as-synthesized materials. FT-IR spectra of the materials showed peak maxima of 1620 cm^{-1} and 1400 cm^{-1} , corresponding to water and ammonium cation in the materials (Figure 2b). The amounts of sodium and ammonium in the materials of Na–Mo–Zn oxide and NH_4 –Mo–Zn oxide were the same (1.5 per one POM unit).

Micropores were constructed by cages and channels, and the cages were connected with the channels in a tetrahedral fashion to build a 3D pore system (Figure 1c). The numbers of cages and channels per one POM were 1 and 2, respectively.

Heat treatment could remove the existing water for Na–Mo–Zn oxide and water and NH_4^+ for NH_4 –Mo–Zn oxide. TPD-MS was applied to investigate desorption of guest

Table 1. Numbers of small molecules per one POM unit adsorbed in the materials at 100 kPa.

| | POM unit | CO ₂ | CH ₄ | C ₂ H ₆ | C ₃ H ₈ |
|-------------------------------------|------------------------------------|-----------------|-----------------|-------------------------------|-------------------------------|
| Cal–Na–Mo–Zn oxide | ZnMo ₁₂ O ₄₀ | 1.84 | 0.86 | 1.04 | 0.11 |
| Cal–NH ₄ –Mo–Zn oxide | ZnMo ₁₂ O ₄₀ | 1.44 | 0.89 | 0.99 | 0.16 |
| Cal–NH ₄ –Na–Mo–Zn oxide | ZnMo ₁₂ O ₄₀ | 1.58 | 0.63 | 0.63 | 0.30 |

$$\text{number of molecule adsorbed} = \frac{\text{adsorbed amount (cm}^3\text{/g)} \times \text{molecule weight of the material (g/mol)}}{22400 \text{ (cm}^3\text{/mol)}}$$

The values were calculated by the equation:

molecules from the as-synthesized materials (Figure S10a,b). The mass numbers m/z of 16 and 18 corresponded to ammonia and water, respectively. In the case of NH₄–Mo–Zn oxide, the TPD-MS profile ($m/z = 16$) revealed only one peak with a peak maxima at 600 K, indicating desorption of ammonia at 600 K. Na–Mo–Zn oxide did not contain any ammonia in the structure. After removal of ammonia from NH₄–Mo–Zn oxide, protons remained in the structure to make charge balance. There were two water desorption peaks, peak maxima of which were at about 400 K and 600 K, in both materials. For Na–Mo–Zn oxide, Na⁺ could not be removed by heating and remained in the structure after heating. TG-DTA profiles indicated the weight loss of the materials during heating. The total weight loss of Na–Mo–Zn oxide was 7.5% and of NH₄–Mo–Zn oxide was 10.7% (Figure S10c,d).

Thermal stability and hydrothermal stability

Thermal stability of the materials was tested. The materials were calcined under N₂ flow (50 mL/min) for 2h at 473 K, 523 K, 573 K, and 623 K (NH₄–Mo–Zn oxide only). The resulting materials were characterized by powder XRD. Na–Mo–Zn oxide was stable at 473 K, and it started to decompose at 523 K as the diffraction peak of (111) decreased dramatically (Figure S11A). Compared with Na–Mo–Zn oxide, NH₄–Mo–Zn oxide was thermally more stable, structure of which did not change at 523 K. Further heating would collapse the structure (Figure S11B).

Hydrothermal stability of the materials was also tested. The material (0.15 g) was dispersed in water (20 mL) followed by introducing the mixture into a 50-mL autoclave, then the autoclave was heated for 24 h at 373 K, 413 K, 448 K, and 503 K in an oven. XRD showed that the peak intensity of both materials almost did not decrease after hydrothermal treatments, indicating that the crystallinity of the materials did not drastically decrease (Figure S11C, D). However, recovery rate of Na–Mo–Zn oxide decreased with increase in the treatment temperature, demonstrating that the material slowly dissolved in water during the hydrothermal treatment (Figure S11E). In the case of NH₄–Mo–Zn oxide, the recovery rate of the material was higher than that of Na–Mo–Zn oxide. The material was stable under the hydrothermal condition below 448 K (Figure S11E).

Both Mo–Zn oxides were thermally stable at 473 K (Figure S11). It was found that calcination at 473 K for 2.5 hours under high vacuum could remove water and NH₃ without collapse of the structure. The remaining guest molecules, water in the calcined material of Na–Mo–Zn oxide (Cal–Na–Mo–Zn oxide) and NH₄⁺ and water in calcined NH₄–Mo–Zn oxide (Cal–NH₄–Mo–Zn oxide), were estimated by TPD measurement (Figure S12). In the case of Na–Mo–Zn oxide, 63% of the water was removed by heating. Heating of NH₄–Mo–Zn oxide removed 41% of the water and 65% of NH₃. The chemical formulas of Cal–NH₄–Mo–Zn oxide and Cal–NH₄–Na–Mo–Zn oxide were estimated to be Na_{1.5}H_{11.4}[Zn^{II}Mo^{VI}_{1.1}Mo^V_{10.9}O₄₀{Zn^{II}₂}]·2H₂O and

(NH₄)_{0.5}H_{9.6}[Zn^{II}Mo^{VI}₄Mo^V₈O₄₀{Zn^{II}₂}]·3.5H₂O, respectively. The amounts of guest species in the two calcined Mo–Zn oxides was similar, 3.5~4 per one POM unit (Table S6).

Adsorption property

N₂ sorption measurements of both calcined oxides showed a sudden N₂ uptake at very low relative pressure ($p/p_0 = 0.001$), indicating that the materials were microporous materials (Figure S13a and Table S7). Pore size distribution calculated by the SF method further demonstrated that both Mo–Zn oxides were microporous materials (Figure S13b). The adsorption properties of Cal–Na–Mo–Zn oxide and Cal–NH₄–Mo–Zn oxide were further studied by small molecule adsorption. The materials selectively adsorbed different kinds of small molecules based on the size of the molecules. Figure 4 shows the adsorption isotherms of CH₄, CO₂, C₂H₆, and C₃H₈ on the materials at 298K. The results indicated that the materials adsorbed small molecules including CH₄, CO₂ and C₂H₆ with kinetic diameters of 0.38, 0.33, and 0.40 nm, respectively, whereas a larger molecule of C₃H₈ with a kinetic diameter of 0.42 nm was not adsorbed by either of the materials.

Surface areas of the materials were calculated by the BET method from CO₂ adsorption isotherms to be 88 m²/g and 68 m²/g for Cal–Na–Mo–Zn oxide and Cal–NH₄–Mo–Zn oxide, respectively. Pore volumes for Cal–Na–Mo–Zn oxide and Cal–NH₄–Mo–Zn oxide were estimated by the DA method⁴⁵ from CO₂ adsorption isotherms to be 0.039 cm³/g and 0.033 cm³/g, respectively. For Cal–Na–Mo–Zn oxide, about 1.84 of CO₂, 0.86 of CH₄, and 1.04 of C₂H₆ per one POM unit were adsorbed. For Cal–NH₄–Mo–Zn oxide, about 1.44 of CO₂, 0.89 of CH₄, and 0.99 of C₂H₆ per one POM unit were adsorbed (Table 1).

Moreover, Mo–Zn oxide with NH₄⁺ was obtained by ion-exchange process (NH₄–Na–Mo–Zn oxide). Here we used high dosage of NH₄Cl to expect to replace all Na⁺ in Na–Mo–Zn oxide. XRD pattern and FT-IR spectra confirmed that the basic structure of NH₄–Na–Mo–Zn oxide was the same as other two Mo–Zn oxide (Figure 2). The appearance of IR band at 1400 cm⁻¹ indicated that NH₄⁺ was successfully introduced into Na–Mo–Zn oxide. Elemental analysis demonstrated there was still Na⁺ in the material and the chemical formula of as-synthesized NH₄–Na–Mo–Zn oxide was (NH₄)_{1.4}Na_{0.1}H_{11.4}[ZnMo₁₂O₄₀{Zn₂}]·5.5H₂O. After calcination at 473 K (denoted as Cal–NH₄–Na–Mo–Zn oxide), TPD-MS (Figure S12d,e) indicated that the chemical formula of the calcined material was (NH₄)_{1.4}Na_{0.1}H_{11.4}[ZnMo₁₂O₄₀{Zn₂}]·3H₂O and most of NH₄⁺ remained.

Molecule adsorption was also carried out on Cal–NH₄–Na–Mo–Zn oxide, showing that the material could also adsorb small molecules (Figure 4). Compared to other two Mo–Zn oxides, the adsorption capacity of Cal–NH₄–Na–Mo–Zn oxide was lower, which might be resulted from remaining NH₄⁺ and water in the Cal–NH₄–Na–Mo–Zn oxide (Table S6). Therefore,

we would like to use Cal-NH₄-Mo-Zn oxide and Cal-Na-Mo-Zn oxide for further experiments.

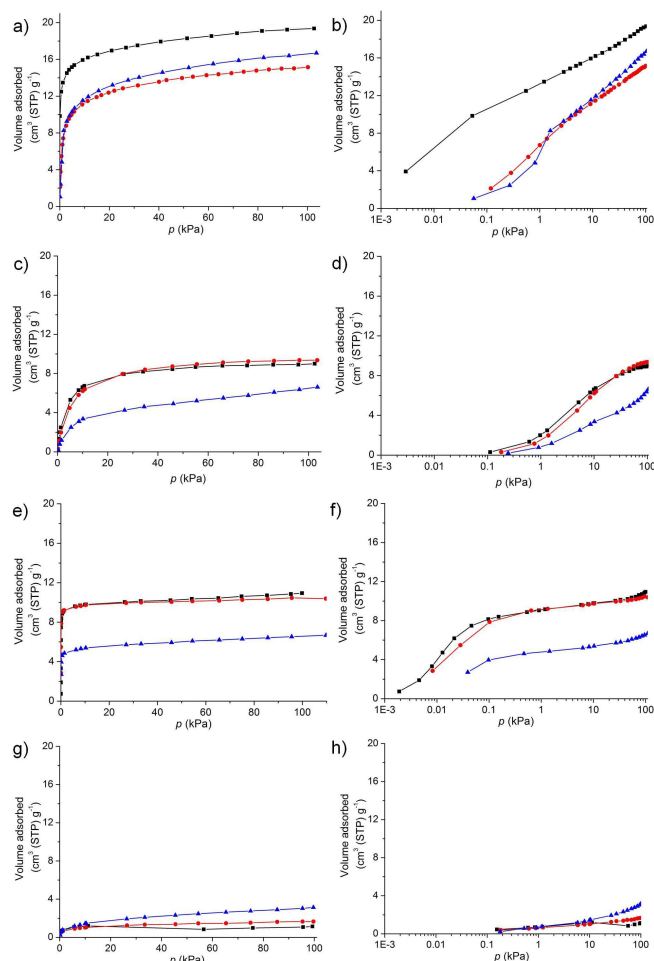


Figure 4. Adsorption isotherms of (a and b) CO₂, (c and d) CH₄, (e and f) C₂H₆, and (g and h) C₃H₈ at 298 K, black: Cal-Na-Mo-Zn oxide, red: Cal-NH₄-Mo-Zn oxide, and blue: Cal-NH₄-Na-Mo-Zn oxide.

CO₂ and CH₄ adsorption. CO₂ uptake in both materials sharply increased in the low pressure range (< 1 kPa), indicating that both Mo-Zn oxides had strong interaction with CO₂, and both materials showed high CO₂ adsorption capacity (19 cm³(STP)/g for Na-Mo-Zn oxide and 15 cm³(STP)/g for Cal-NH₄-Mo-Zn oxide at 100 kPa (Figure 4a,b). In the case of CH₄ adsorption, the molecule uptake in the low pressure range increased gradually, indicating that the materials showed weaker interaction with CH₄ than that with CO₂ (Figure 4c,d). Both calcined Mo-Zn oxides adsorbed CO₂ at a low pressure (< 1 kPa), whereas they could not adsorb CH₄ at such a low pressure.

The enthalpy of adsorption by calculated with the Clausius-Clapeyron equation, which is shown in Figure 5. The enthalpy of CO₂ and CH₄ adsorption for Na-Mo-Zn oxide was calculated to be 46~65 kJ/mol and 18~30 kJ/mol, respectively. The enthalpy of CO₂ and CH₄ adsorption for NH₄-Mo-Zn oxide was calculated to be 35~45 kJ/mol and 25~30 kJ/mol, respectively. The enthalpy of CO₂ adsorption in both materials was higher than that of CH₄ adsorption, indicating that the materials strongly interacted with CO₂ but weakly interacted with CH₄.

CO₂ adsorption isotherms of Cal-Na-Mo-Zn oxide and Cal-NH₄-Mo-Zn oxide were different. Cal-Na-Mo-Zn oxide showed much higher adsorption capacity than that of Cal-NH₄-Mo-Zn oxide not only at a high pressure but also at a low pressure (< 1 kPa), at which adsorption in micropores occurred (Figure 4a,b). The enthalpy of CO₂ adsorption (Figure 5) for Cal-Na-Mo-Zn oxide (46~65 kJ/mol) appeared to be higher than that of CO₂ for Cal-NH₄-Mo-Zn oxide (35~45 kJ/mol), indicating that Na⁺ in Cal-Na-Mo-Zn oxide showed stronger interaction with CO₂ than did proton or ammonium cation in Cal-NH₄-Mo-Zn oxide.

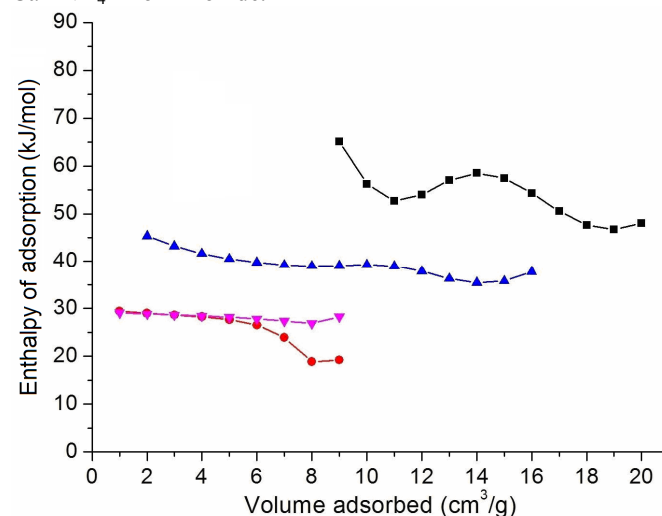


Figure 5. Enthalpy of CO₂ and CH₄ adsorption for Cal-Na-Mo-Zn oxide and Cal-NH₄-Mo-Zn oxide, black: Cal-Na-Mo-Zn oxide adsorbed CO₂, red: Cal-Na-Mo-Zn oxide adsorbed CH₄, blue: Cal-NH₄-Mo-Zn oxide adsorbed CO₂, purple: Cal-NH₄-Mo-Zn oxide adsorbed CH₄.

On the other hand, adsorption isotherms of CH₄ in Cal-Na-Mo-Zn oxide and Cal-NH₄-Mo-Zn oxide were almost the same. For both calcined Mo-Zn oxides, about 10 cm³/g of gas molecule was adsorbed at 298 K and at 100 kPa. Enthalpy of CH₄ adsorption for Cal-Na-Mo-Zn oxide (18~30 kJ/mol) and that for Cal-NH₄-Mo-Zn oxide (25~30 kJ/mol) was almost the same. Therefore, Na⁺ did not affect the adsorption of CH₄ in the materials.

It was reported that the electronic properties of CO₂ and CH₄ caused the different adsorption behaviors. CO₂ has a large quadrupole moment (13.4×10⁻⁴⁰ Cm²), whereas CH₄ is non-polar.⁴⁶ The large amount of CO₂ adsorption and the strong interaction of CO₂ with frameworks were attributed to large quadrupole moment of CO₂ molecule,⁴⁷ which resulted in a relatively strong attraction to the electrostatic field of frameworks.⁴⁸ Cation species would have influence on the adsorption of CO₂. The effect of a cation is complicated. In some reports, it was claimed that the enhancement of CO₂ adsorption after introducing alkaline metal ions is due to increase in the basicity of the material.⁴⁸ In other reports, this was ascribed to alkaline metal ions with high positive atomic partial charge, which strongly interacted with CO₂.⁴⁹

In the present study, partial atomic charges of Na-Mo-Zn oxide and NH₄-Mo-Zn oxide were analyzed by DFT calculations, and the results are shown in Table S8 and Table S9. Frameworks of the materials were covered with oxygen atoms that were all negatively charged. Countercations such as proton and Na⁺ in the material were positively charged. This framework would display an electrostatic field, and therefore

CO₂ would have stronger electrostatic interaction than CH₄ with the framework. Furthermore, the atomic charge of Na⁺ was much higher than that of proton in the material, indicating stronger interaction between Na⁺ and CO₂.

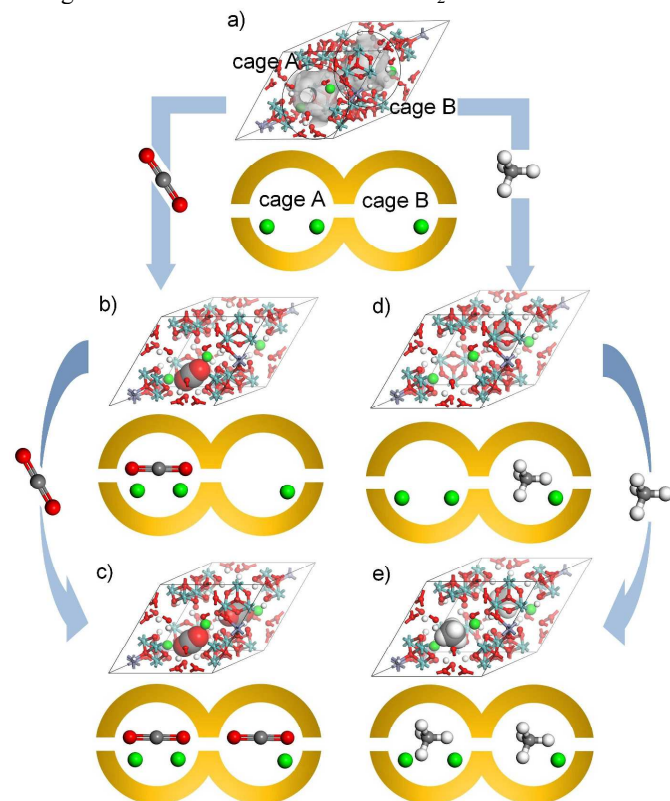


Figure 6. Representations of adsorbed structures of Cal-Na-Mo-Zn oxide from Monte Carlo simulation, upper: ball-and-stick representations, lower: schematic representations. a) primitive cell with cage A and cage B, b) Cal-Na-Mo-Zn oxide adsorbed first CO₂, c) Cal-Na-Mo-Zn oxide adsorbed second CO₂, d) Cal-Na-Mo-Zn oxide adsorbed first CH₄, and e) Cal-Na-Mo-Zn oxide adsorbed second CH₄, blue sphere: Mo, purple sphere: Zn, red sphere: O, white sphere: H, gray sphere: C, and green sphere: Na.

Monte Carlo simulation. A primitive cell of Cal-Na-Mo-Zn oxide contained 2 POM units of [ZnMo₁₂O₄₀] with 2 cages, 23 protons and 3 Na⁺. Assuming that Na⁺ were located in two cages of the material, one cage contains two Na⁺ (cage A) and another cage contains the other Na⁺ (cage B) (Figure 6a). Monte Carlo simulation was performed on Cal-Na-Mo-Zn oxide to estimate affinity of CO₂ with Na⁺. CO₂ was loaded one by one during the simulation. It was found that the first CO₂ was located in cage A and the second CO₂ was located in cage B (Figure 6b and c). In cage A, these two Na ions were bridged by CO₂ in a $\mu\text{-}\eta^1\text{-}\eta^1$ fashion, as shown in Figure 6b and 6c. The

distance between the Na⁺ and the carbon atoms of CO₂ was calculated to be 2.35 Å, indicating that CO₂ strongly interacted with Na⁺ in cage A. Adsorption energies estimated by Monte Carlo simulation for CO₂ in cage A (Figure 6b) and CO₂ in cage B (Figure 6c) were 53 and 41 kJ/mol, respectively. The results of calculation were consistent with the observed trend of adsorption enthalpy of CO₂ in the material. In the case of CH₄, CH₄ was firstly filled in cage B, because cage B had more space and CH₄ had weak electrostatic interaction with Na⁺ (Figure 6d and e). Adsorption energies from Monte Carlo simulation for CH₄ in both sites were 24 kJ/mol, also indicating that CH₄ would weakly interacted with Na⁺.

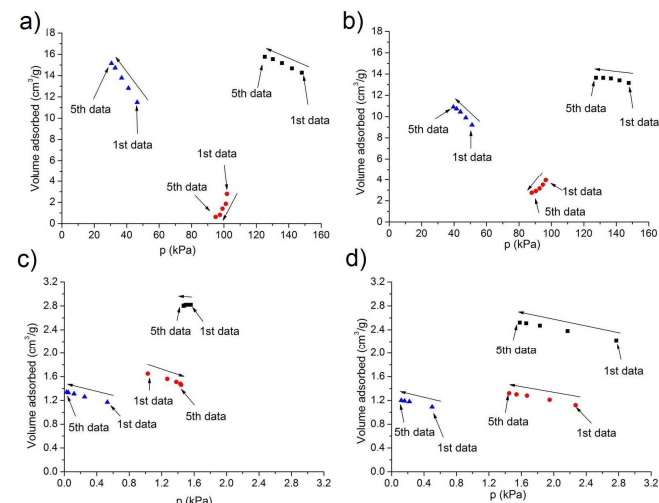


Figure 7. CO₂/CH₄ co-sorption results of a) Cal-Na-Mo-Zn oxide at high pressure, b) Cal-NH₄-Mo-Zn oxide at high pressure, c) Cal-Na-Mo-Zn oxide at low pressure, and d) Cal-NH₄-Mo-Zn oxide at low pressure, black square: system total pressure (x-axis) and adsorbed amount (y-axis), red cycle: CH₄ partial pressure (x-axis) and adsorbed amount (y-axis), blue triangle: CO₂ partial pressure (x-axis) and adsorbed amount (y-axis).

Co-sorption and separation experiment. CO₂ exists widely in landfill gas. CO₂ selective adsorption from a CO₂/CH₄ mixture is of great importance for improvement of gas quality. Co-adsorption experiments were carried out on Cal-Na-Mo-Zn oxide and Cal-NH₄-Mo-Zn oxide under both high pressures (125.2 and 127.5 kPa of equilibrium total pressures) and low pressures (1.5 and 1.6 kPa of equilibrium total pressures) at 298 K. The initial ratio of CO₂ and CH₄ was 40: 60, a typical composition of biogas.⁵⁰ According to the individual adsorption isotherms, in the low pressure range, the materials might show high separation efficiency of CO₂.

Equilibrium total pressure, total adsorbed amount, CO₂

Table 2. CO₂/CH₄ co-sorption in the materials.

| entry | Material | p_e (kPa) ^b | ratio in gas phase (%) | | ratio in adsorbed phase (%) | | CO ₂ selectivity |
|-------|----------------------------------|-----------------------------|------------------------|-----------------|-----------------------------|-----------------|-----------------------------|
| | | | CO ₂ | CH ₄ | CO ₂ | CH ₄ | |
| 1 | Cal-Na-Mo-Zn oxide | 1.5 | 1.70 | 98.3 | 47.4 | 52.6 | 52 |
| 2 | Cal-Na-Mo-Zn oxide | 125.2 | 24.4 | 75.6 | 96.0 | 4.0 | 75 |
| 3 | Cal-NH ₄ -Mo-Zn oxide | 1.6 | 7.80 | 92.2 | 47.7 | 52.3 | 11 |
| 4 | Cal-NH ₄ -Mo-Zn oxide | 127.5 | 31.0 | 69.0 | 79.8 | 20.2 | 9 |

^a These are 5th equilibrium data. ^b p_e denotes the equilibrium total pressure.

and CH₄ partial pressures, and CO₂ and CH₄ adsorbed amounts are shown in Figure 7. In the high pressure condition, both materials adsorbed more CO₂ than CH₄. When the materials continued to be left under mixed gas pressure, they further adsorbed CO₂, while CH₄ desorbed from the materials (Figure 7a,b), indicating that adsorbed CH₄ was partly replaced by CO₂. Moreover, Cal–Na–Mo–Zn oxide (15 cm³/g at the fifth co-sorption equilibrium) tended to adsorb more CO₂ than did Cal–NH₄–Mo–Zn oxide (11 cm³/g at the fifth co-sorption equilibrium). In the low pressure condition, the two materials adsorbed similar amounts of CO₂ and CH₄. With prolongation of the adsorption process, Cal–Na–Mo–Zn oxide further adsorbed CO₂ and concurrently desorbed CH₄, while Cal–NH₄–Mo–Zn oxide adsorbed both CH₄ and CO₂ (Figure 7c,d).

CO₂ selectivity of the final equilibrium (5th equilibrium data in Figure 7) for the material was calculated and summarized in Table 2. Cal–Na–Mo–Zn oxide showed higher selectivity of CO₂ adsorption than that of Cal–NH₄–Mo–Zn oxide under both high and low pressure conditions. Co-sorption experiments demonstrated that Cal–Na–Mo–Zn oxide had better performance of CO₂ separation than that of Cal–NH₄–Mo–Zn oxide.

Table S10 summarize the performance of different adsorbents, such as zeolites, MOF materials, and other porous materials, for CO₂ selective adsorption from CO₂/CH₄ mixture. CO₂ selectivity of Cal–Na–Mo–Zn oxide was higher than the reported materials in Table S10, which indicated that Cal–Na–Mo–Zn oxide was a good candidate for CO₂ selective adsorption and separation.

Furthermore, Cal–Na–Mo–Zn oxide was successfully applied to GC separation of CO₂ from a CO₂/CH₄ mixture. The gas mixture (CO₂: CH₄ = 1: 1) was injected into a gas chromatograph equipped with a column filled with Na–Mo–Zn oxide. As shown in Figure 8, CH₄ and CO₂ were separated within a few minutes at 363 K. The peak of CO₂ appeared slower and was broader than that of CH₄, indicating that the material had stronger interaction with CO₂ than with CH₄.

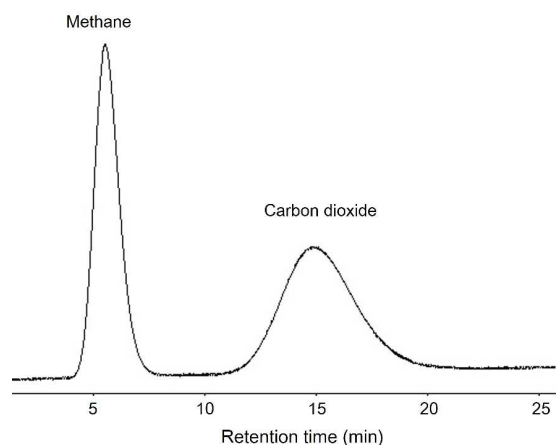


Figure 8. Gas chromatograms of a gas mixture of CO₂ and CH₄ separated on a column of Cal–Na–Mo–Zn oxide.

Conclusion

The materials of Cal–Na–Mo–Zn oxide and Cal–NH₄–Mo–Zn oxide adsorbed small molecules including CO₂, C₂H₆, and CH₄. Both oxides selectively adsorbed CO₂ from the CO₂/CH₄ mixture, because the materials showed higher adsorption capacity of CO₂ than that of CH₄. Cal–Na–Mo–Zn oxide showed stronger interaction with CO₂ than Cal–NH₄–Mo–Zn oxide did, while both oxides showed similar interactions with CH₄. Co-sorption experiments showed that selectivity of CO₂ on Na–Mo–Zn oxide was higher than that on Cal–NH₄–Mo–Zn oxide. Cal–Na–Mo–Zn oxide was applied to GC separation, and CO₂ could be efficiently separated from the CO₂/CH₄ mixture by using the material.

Acknowledgements

This work was financially supported by a Grant-in-Aid for Scientific Research (A) (grant No. 2324-6135) from the Ministry of Education, Culture, Sports, Science, and Technology, Japan. M. S. thanks PRESTO, JST and Nippon Sheet Glass Foundation for Materials Science and Engineering (NSG Foundation) for financial support. S. N. Thanks a Grant-in-Aid for Science Research from the Ministry of Education, Culture, Sports, Science and Technology, Japan (Grant No. 24550068). K. Y. thanks Grants-in-Aid (Grant Nos. 22245028 and 24109014) for Scientific Research from JSPS and MEXT and the MEXT Projects of “Integrated Research on Chemical Synthesis” and “Elements Strategy Initiative for Catalysts and Batteries”.

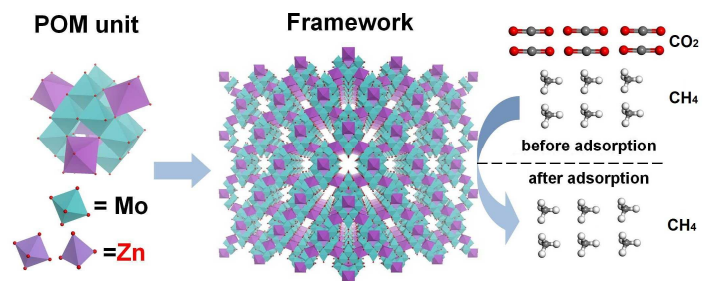
Notes and references

- ¹ Catalysis Research Center, Hokkaido University, N-21, W-10, Kita-ku, Sapporo 001-0021, Japan.
 - ² Department of Applied Chemistry, Graduate School of Engineering, Hiroshima University, 1-4-1 Kagamiyama, Higashi Hiroshima 739-8527, Japan.
 - ³ JST, PRESTO, 4-1-8 Honcho, Kawaguchi, Saitama 332-0012, Japan.
 - ⁴ Research Institute for Electronic Science, Hokkaido University, Sapporo 001-0020, Japan.
 - ⁵ Creative Research Institute (CRIS), Hokkaido University, Sapporo 001-0021, Japan.
 - ⁶ Institute for Materials Chemistry and Engineering and International Research Center for Molecular Systems, Kyushu University, Fukuoka 819-0395, Japan
- *E-mail: ueda@cat.hokudai.ac.jp. Phone: +81-11-706-9164. Fax: +81-11-706-9163.

Electronic Supplementary Information (ESI) available: [details of any supplementary information available should be included here]. See DOI: 10.1039/b000000x/

1. G. Férey, C. Serre, T. Devic, G. Maurin, H. Jobic, P. L. Llewellyn, G. De Weireld, A. Vimont, M. Daturi, and J.-S. Chang, *Chem. Soc. Rev.*, 2011, **40**, 550–562.
2. K. Sumida, D. L. Rogow, J. a Mason, T. M. McDonald, E. D. Bloch, Z. R. Herm, T.-H. Bae, and J. R. Long, *Chem. Rev.*, 2012, **112**, 724–781.
3. N. Du, H. B. Park, M. M. Dal-Cin, and M. D. Guiver, *Energy Environ. Sci.*, 2012, **5**, 7306–7322.
4. N. A. Khan, Z. Hasan, and S. H. Jhung, *J. Hazard. Mater.*, 2013, **244-245**, 444–456.
5. A. M. Kierzkowska, R. Pacciani, and C. R. Müller, *ChemSusChem*, 2013, **6**, 1130–1148.

6. Y. Kamiya, M. Sadakane, W. Ueda, and J. Reedijk Poepfelmeier, K., Heteropoly Compounds in *Comprehensive Inorganic Chemistry II*, Oxford: Elsevier, 2013, vol. 7.
7. Special thematic issue on polyoxometalates. Hill, C. L.; Ed.; *Chem. Rev.*, 1998, **98**, 1–390.
8. Special thematic issue on polyoxometalates. Cronin, L.; Müller, A.; Ed.; *Chem. Soc. Rev.*, 2012, **41**, 7325–7648.
9. D.-L. Long, R. Tsunashima, and L. Cronin, *Angew. Chem., Int. Ed.*, 2010, **49**, 1736–1758.
10. M. Sadakane, K. Kodato, T. Kuranishi, Y. Nodasaka, K. Sugawara, N. Sakaguchi, T. Nagai, Y. Matsui, and W. Ueda, *Angew. Chem., Int. Ed.*, 2008, **47**, 2493–2496.
11. M. Sadakane, K. Yamagata, K. Kodato, K. Endo, K. Toriumi, Y. Ozawa, T. Ozeki, T. Nagai, Y. Matsui, N. Sakaguchi, W. D. Pyrz, D. J. Buttrey, D. A. Blom, T. Vogt, and W. Ueda, *Angew. Chem., Int. Ed.*, 2009, **48**, 3782–3786.
12. M. Sadakane, N. Watanabe, T. Katou, Y. Nodasaka, and W. Ueda, *Angew. Chem., Int. Ed.*, 2007, **46**, 1493–1496.
13. S. G. Mitchell, C. Streb, H. N. Miras, T. Boyd, D.-L. Long, and L. Cronin, *Nat. Chem.*, 2010, **2**, 308–312.
14. D. Liu, Y. Lu, H.-Q. Tan, W.-L. Chen, Z.-M. Zhang, Y.-G. Li, and E.-B. Wang, *Chem. Commun.*, 2013, 3673–3675.
15. A. Dolbecq, C. Mellot-Draznieks, P. Mialane, J. Marrot, G. Férey, and F. Sécheresse, *Eur. J. Inorg. Chem.*, 2005, 3009–3018.
16. G. Férey, C. Mellot-Draznieks, C. Serre, F. Millange, J. Dutour, S. Surblé, and I. Margiolaki, *Science*, 2005, **309**, 2040–2042.
17. L. M. Rodriguez-Albelo, A. Rabdel Ruiz-Salvador, A. Sampieri, D. W. Lewis, A. Gomez, B. Nohra, P. Mialane, J. Marrot, F. Secheresse, C. Mellot-Draznieks, R. N. Biboum, B. Keita, L. Nadjo, and A. Dolbecq, *J. Am. Chem. Soc.*, 2009, **131**, 16078–16087.
18. J. Song, Z. Luo, D. K. Britt, H. Furukawa, O. M. Yaghi, K. I. Hardcastle, and C. L. Hill, *J. Am. Chem. Soc.*, 2011, **133**, 16839–16846.
19. C.-Y. Sun, S.-X. Liu, D.-D. Liang, K.-Z. Shao, Y.-H. Ren, and Z.-M. Su, *J. Am. Chem. Soc.*, 2009, **131**, 1883–1888.
20. B. Nohra, H. El Moll, L. M. Rodriguez Albelo, P. Mialane, J. Marrot, C. Mellot-Draznieks, M. O’Keeffe, R. N. Biboum, J. Lemaire, B. Keita, L. Nadjo, and A. Dolbecq, *J. Am. Chem. Soc.*, 2011, **133**, 13363–13374.
21. H. Tagami, S. Uchida, and N. Mizuno, *Angew. Chem., Int. Ed.*, 2009, **48**, 6160–6164.
22. S. Uchida, R. Eguchi, and N. Mizuno, *Angew. Chem., Int. Ed.*, 2010, **49**, 9930–9934.
23. S. Uchida, M. Hashimoto, and N. Mizuno, *Angew. Chem., Int. Ed.*, 2002, **6**, 2814–2817.
24. R. Eguchi, S. Uchida, and N. Mizuno, *Angew. Chem., Int. Ed.*, 2012, **51**, 1635–1639.
25. N. Mizuno and S. Uchida, *Chem. Lett.*, 2006, **35**, 688–693.
26. S. Uchida, S. Hikichi, T. Akatsuka, T. Tanaka, R. Kawamoto, A. Lesbani, Y. Nakagawa, K. Uehara, and N. Mizuno, *Chem. Mater.*, 2007, **19**, 4694–4701.
27. R. Eguchi, S. Uchida, and N. Mizuno, *J. Phys. Chem. C*, 2012, **116**, 16105–16110.
28. Y. Ogasawara, S. Uchida, and N. Mizuno, *J. Phys. Chem. C*, 2007, **6**, 8218–8227.
29. S. Uchida and N. Mizuno, *J. Am. Chem. Soc.*, 2004, **6**, 1602–1603.
30. Z. Zhang, M. Sadakane, T. Murayama, S. Izumi, N. Yasuda, N. Sakaguchi, and W. Ueda, *Inorg. Chem.*, 2014, **53**, 903–911.
31. Z. Zhang, M. Sadakane, T. Murayama, and W. Ueda, *Dalt. Trans.*, 2014, **43**, 13584–13590.
32. Z. Zhang, M. Sadakane, T. Murayama, N. Sakaguchi, and W. Ueda, *Inorg. Chem.*, 2014, **53**, 7309–7318.
33. A. L. McClellan and H. F. Harnsberger, *J. Colloid Interface Sci.*, 1967, **23**, 577–599.
34. W. i. f. David, K. Shankland, L. b. McCusker, and C. Baerlocher, Eds., *Structure Determination from Powder Diffraction Data*, Oxford University Press, 2006, vol. 47.
35. M. A. Neumann, *J. Appl. Crystallogr.*, 2003, **36**, 356–365.
36. R. A. Young, *The Rietveld Method*, Oxford University Press, Oxford, 1995.
37. A. Boulton and D. Louer, *J. Appl. Crystallogr.*, 2004, **37**, 724–731.
38. L. Palatinus and G. Chapuis, *J. Appl. Crystallogr.*, 2007, **40**, 786–790.
39. B. Delley, *J. Chem. Phys.*, 2000, **113**, 7759–7764.
40. B. Delley, *J. Chem. Phys.*, 1990, **92**, 508–517.
41. E. D. Akten, R. Siriwardane, and D. S. Sholl, *Energy & Fuels*, 2003, **17**, 977–983.
42. T. R. Zeitler, M. D. Allendorf, and A. Greathouse, *J. Phys. Chem. C*, 2012, **116**, 3492–3502.
43. X. Li, Z. Wang, J. Zheng, S. Shao, Y. Wang, and Y. Yan, *Chinese J. Catal.*, 2011, **32**, 217–223.
44. S. Aguado, J. Gascón, J. C. Jansen, and F. Kapteijn, *Microporous Mesoporous Mater.*, 2009, **120**, 170–176.
45. M. M. Dubinin, *Prog. Surf. Membr. Sci.*, 1975, **9**, 1–70.
46. D. M. D’Alessandro, B. Smit, and J. R. Long, *Angew. Chem., Int. Ed.*, 2010, **49**, 6058–6082.
47. J. Zhang, N. Burke, S. Zhang, K. Liu, and M. Pervukhina, *Chem. Eng. Sci.*, 2014, **113**, 54–61.
48. X. Xu, X. Zhao, L. Sun, and X. Liu, *J. Nat. Gas Chem.*, 2008, **17**, 391–396.
49. A. Zukal, J. Mayerová, and J. Čejka, *Phys. Chem. Chem. Phys.*, 2010, **12**, 5240–5247.
50. X. Zhu, K. Li, J.-L. Liu, X.-S. Li, and A.-M. Zhu, *Int. J. Hydrogen Energy*, 2014, **39**, 13902–13908.



The new ϵ -Keggin POM-based frameworks effectively separate CO₂ from CO₂/CH₄ mixture.